

**Critical behavior of quasi-two-dimensional semiconducting ferromagnet  $\text{Cr}_2\text{Ge}_2\text{Te}_6$** 

Yu Liu (刘育) and C. Petrovic

*Condensed Matter Physics and Materials Science Department, Brookhaven National Laboratory, Upton, New York 11973, USA*

(Received 16 June 2017; published 3 August 2017; corrected 29 November 2018 and 14 January 2020)

The critical properties of the single-crystalline semiconducting ferromagnet  $\text{Cr}_2\text{Ge}_2\text{Te}_6$  were investigated by bulk dc magnetization around the paramagnetic to ferromagnetic phase transition. Critical exponents  $\beta = 0.200 \pm 0.003$  with a critical temperature  $T_c = 62.65 \pm 0.07$  K and  $\gamma = 1.28 \pm 0.03$  with  $T_c = 62.75 \pm 0.06$  K are obtained by the Kouvel-Fisher method whereas  $\delta = 7.96 \pm 0.01$  is obtained by a critical isotherm analysis at  $T_c = 62.7$  K. These critical exponents obey the Widom scaling relation  $\delta = 1 + \gamma/\beta$ , indicating self-consistency of the obtained values. With these critical exponents the isotherm  $M(H)$  curves below and above the critical temperatures collapse into two independent universal branches, obeying the single scaling equation  $m = f_{\pm}(h)$ , where  $m$  and  $h$  are renormalized magnetization and field, respectively. The determined exponents match well with those calculated from the results of the renormalization group approach for a two-dimensional Ising system coupled with a long-range interaction between spins decaying as  $J(r) \approx r^{-(d+\sigma)}$  with  $\sigma = 1.52$ .

DOI: [10.1103/PhysRevB.96.054406](https://doi.org/10.1103/PhysRevB.96.054406)**I. INTRODUCTION**

Two-dimensional (2D) materials have recently stimulated significant attention not only for the emergence of novel properties but also for potential applications [1–5]. In particular, layered intrinsically ferromagnetic (FM) semiconductors are of great interest since both ferromagnetism and semiconducting character are of interest for next-generation spintronic devices [6–11].  $\text{Cr}_2\text{X}_2\text{Te}_6$  ( $X = \text{Si}, \text{Ge}$ ) crystals belong to this class; they have an optical band gap of 0.4 eV for  $\text{Cr}_2\text{Si}_2\text{Te}_6$  or 0.7 eV for  $\text{Cr}_2\text{Ge}_2\text{Te}_6$  [5,10], and simultaneously exhibit ferromagnetic ordering below a Curie temperature ( $T_c$ ) of 32 K for  $\text{Cr}_2\text{Si}_2\text{Te}_6$  or 61 K for  $\text{Cr}_2\text{Ge}_2\text{Te}_6$ , respectively [10–15].

Considerable efforts have been devoted in order to shed light on the nature of ferromagnetism in bulk and monolayer  $\text{Cr}_2\text{X}_2\text{Te}_6$  [16–20]. Previous neutron scattering showed that bulk  $\text{Cr}_2\text{Si}_2\text{Te}_6$  is a strongly anisotropic 2D Ising-like ferromagnet with a critical exponent  $\beta = 0.17$  and a spin gap of  $\sim 6$  meV [21]. The critical behavior of  $\text{Cr}_2\text{Si}_2\text{Te}_6$  investigated by bulk magnetization measurements further confirms the critical exponent  $\beta = 0.170 \pm 0.008$ , comparable to  $\beta = 0.125$  for a 2D Ising model [22]. However, recent neutron work on  $\text{Cr}_2\text{Si}_2\text{Te}_6$  observed  $\beta = 0.151$  and a very small spin gap of  $\sim 0.075$  meV [23]. Based on a spin wave analysis, the spins in  $\text{Cr}_2\text{Si}_2\text{Te}_6$  are Heisenberg-like [23]. The spin wave theory also suggests that  $\text{Cr}_2\text{Ge}_2\text{Te}_6$  is a nearly ideal 2D Heisenberg ferromagnet [4]. On the theoretical side, Monte Carlo simulations based on a Heisenberg model predict robust 2D ferromagnetism that exists in nanosheets of a single  $\text{Cr}_2\text{X}_2\text{Te}_6$  layer with  $T_c \sim 35.7$  K for  $\text{Cr}_2\text{Si}_2\text{Te}_6$  or  $\sim 57.2$  K for  $\text{Cr}_2\text{Ge}_2\text{Te}_6$  [16], which can also be regarded as the theoretical prediction of corresponding bulk systems since only the nearest-neighbor (NN) exchange is considered. The predicted Curie temperatures are in good agreement with the experimental ones [12,13]. By further applying a moderate tensile strain, 2D ferromagnetism is predicted theoretically to be largely enhanced with  $T_c$  increasing to  $\sim 91.7$  K for  $\text{Cr}_2\text{Si}_2\text{Te}_6$  or  $\sim 108.9$  K for  $\text{Cr}_2\text{Ge}_2\text{Te}_6$ , respectively [16]. However, the Mermin-Wagner theorem states that long-range ferromagnetic order should not exist at a nonzero temperature based on a 2D isotropic Heisenberg model [24], with the

exception that the spins in the 2D system are constrained to only one direction, i.e., Ising-like spins [25]. Sivasdas *et al.* claimed that when the second and third NN exchange interactions are considered, the monolayer  $\text{Cr}_2\text{Si}_2\text{Te}_6$  is expected to be an antiferromagnet with a zigzag spin texture whereas  $\text{Cr}_2\text{Ge}_2\text{Te}_6$  is still a ferromagnet with a  $T_c$  of 106 K [18]. This is in contrast with a previous result where only the NN exchange interaction was considered [16]. It is also predicted that monolayer  $\text{Cr}_2\text{Si}_2\text{Te}_6$  can be made ferromagnetic with a  $T_c$  of 111 K when applying a moderate uniform in-plane tensile strain of  $\sim 3\%$ , which is experimentally feasible [18]. However, a recent scanning magneto-optic Kerr microscopy experiment on  $\text{Cr}_2\text{Ge}_2\text{Te}_6$  shows that  $T_c$  monotonically decreases with decreasing thickness, from a bulk of about 68 K to a bilayer value of about 30 K [4], which is in contrast to the theoretical prediction.

In order to clarify the magnetic behavior in few-layer samples and the possible applications of this material, it is necessary to establish the nature of magnetism in the bulk. In this paper, we investigate the critical behavior of  $\text{Cr}_2\text{Ge}_2\text{Te}_6$  by various techniques, such as a modified Arrott plot, Kouvel-Fisher plot, and critical isotherm analysis. Our analyses indicate that the obtained critical exponents  $\beta = 0.200 \pm 0.003$  ( $T_c = 62.65 \pm 0.07$  K),  $\gamma = 1.28 \pm 0.03$  ( $T_c = 62.75 \pm 0.06$  K), and  $\delta = 7.96 \pm 0.01$  ( $T_c = 62.7$  K) are in good agreement with those calculated from the results of the renormalization group approach for a 2D Ising model coupled with a long-range interaction between spins decaying as  $J(r) \approx r^{-(d+\sigma)}$  with  $\sigma = 1.52$ .

**II. EXPERIMENTAL DETAILS**

High-quality  $\text{Cr}_2\text{Ge}_2\text{Te}_6$  single crystals were grown by the self-flux technique starting from an intimate mixture of pure elements Cr (99.95%, Alfa Aesar) powder, Ge (99.999%, Alfa Aesar) pieces, and Te (99.9999%, Alfa Aesar) pieces with a molar ratio of 1 : 2 : 6. The starting materials were sealed in an evacuated quartz tube, which was heated to 1100 °C over 20 h, held at 1100 °C for 3 h, and then slowly cooled to 700 °C at a rate of 1 °C/h. X-ray diffraction (XRD) data were

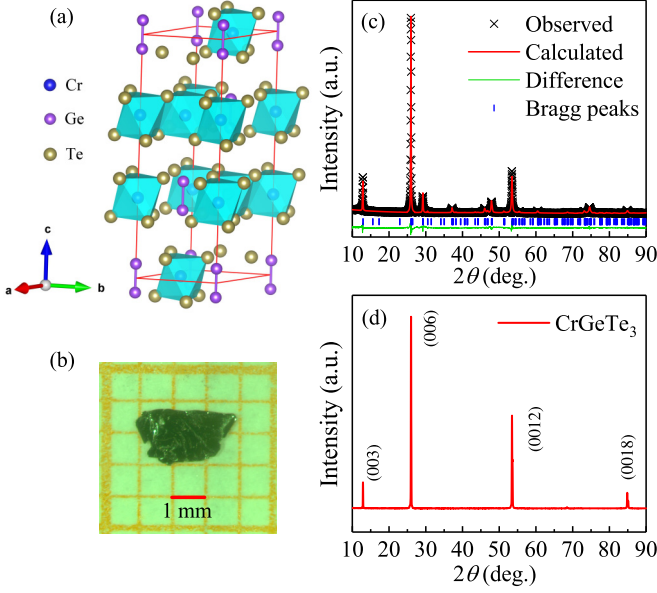


FIG. 1. (a) Crystal structure of  $\text{Cr}_2\text{Ge}_2\text{Te}_6$ . (b) Image of a representative single-crystalline sample. (c) Powder x-ray diffraction (XRD) and (d) single-crystal XRD pattern of  $\text{Cr}_2\text{Ge}_2\text{Te}_6$ . The vertical tick marks represent Bragg reflections of the  $R\bar{3}h$  space group.

taken with  $\text{Cu } K\alpha$  ( $\lambda = 0.15418 \text{ nm}$ ) radiation of a Rigaku Miniflex powder diffractometer. The element analysis was performed using energy-dispersive x-ray spectroscopy (EDX) in a JEOL LSM-6500 scanning electron microscope. The magnetization was measured in a Quantum Design magnetic property measurement system (MPMS-XL5). Isotherms were collected at an interval of 0.5 K around  $T_c$ . The applied magnetic field ( $H_a$ ) has been corrected for the internal field as  $H = H_a - NM$ , where  $M$  is the measured magnetization and  $N$  is the demagnetization factor. The corrected  $H$  was used for the analysis of critical behavior.

### III. RESULTS AND DISCUSSIONS

Bulk  $\text{Cr}_2\text{Ge}_2\text{Te}_6$  is a well-known semiconducting ferromagnet, which was first synthesized by Carreau *et al.* [13]. Figure 1(a) shows the crystal structure of  $\text{Cr}_2\text{Ge}_2\text{Te}_6$ . Each unit cell comprises three  $\text{Cr}_2\text{Ge}_2\text{Te}_6$  layers stacked in an  $ABC$  sequence along the  $c$  axis. The Cr ions are located at the centers of slightly distorted octahedra of Te atoms. The Ge pairs form  $\text{Ge}_2\text{Te}_6$  ethanelike groups. The as-grown single crystals are platelike, typically 3–4 mm in size, as shown in Fig. 1(b). Figure 1(c) presents the powder x-ray diffraction (XRD) pattern of  $\text{Cr}_2\text{Ge}_2\text{Te}_6$ , in which the observed peaks are well fitted with the  $R\bar{3}h$  space group. The determined lattice parameters are  $a = 6.826(2) \text{ \AA}$  and  $c = 20.531(2) \text{ \AA}$ , which are very close to the values reported previously [5,13]. Furthermore, in the single-crystal  $2\theta$  XRD scan [Fig. 1(d)], only (00 $l$ ) peaks are detected, indicating the crystal surface is normal to the  $c$  axis with the plate-shaped surface parallel to the  $ab$  plane.

Figure 2(a) shows the temperature dependence of magnetization  $M(T)$  measured under  $H = 1 \text{ kOe}$  applied in the  $ab$  plane and parallel to the  $c$  axis, respectively. A clear paramagnetic (PM) to ferromagnetic (FM) transition is observed and

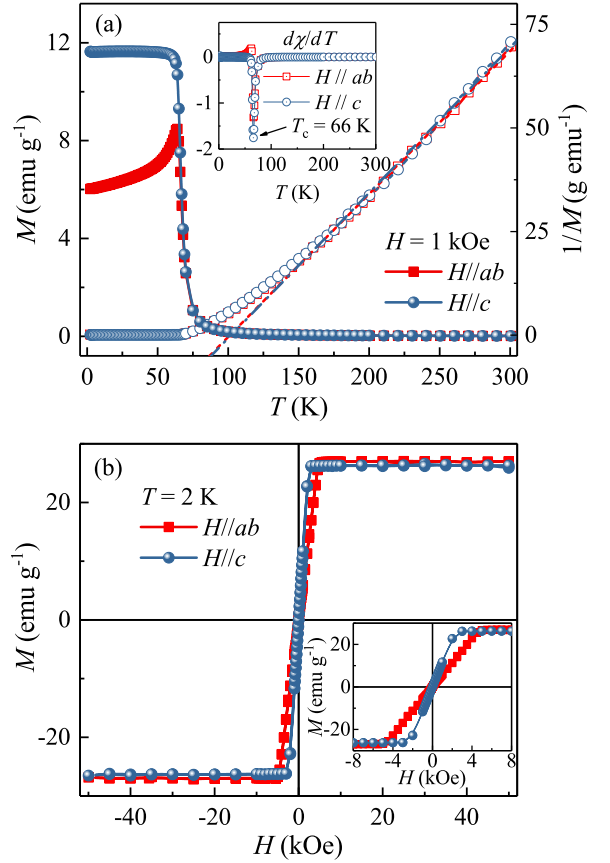


FIG. 2. (a) Temperature dependence of magnetization for  $\text{Cr}_2\text{Ge}_2\text{Te}_6$  measured in the magnetic field  $H = 1 \text{ kOe}$ . Inset: The derivative magnetization  $dM/dT$  vs  $T$ . (b) Field dependence of magnetization for  $\text{Cr}_2\text{Ge}_2\text{Te}_6$  measured at  $T = 2 \text{ K}$ . Inset: The magnification of the low-field region.

the apparent anisotropy suggests that the crystallographic  $c$  axis is the easy axis. As shown in the inset of Fig. 2(a), the critical temperature  $T_c \approx 66 \text{ K}$  is roughly determined from the minimum of the  $dM/dT$  curve, which is in good agreement with the value reported previously [5,13]. The temperature dependence of  $1/M$  is also plotted in Fig. 2(a). A linear fit of the  $1/M$  data in the temperature range of 150–300 K yields the Weiss temperature  $\theta_{ab} \approx 108(1) \text{ K}$  or  $\theta_c \approx 113(2) \text{ K}$ , which is nearly twice the value of  $T_c$ , indicating a strong FM interaction. The effective moment  $\mu_{\text{eff}} = 3.43(2)\mu_B/\text{Cr}$  obtained from  $H \parallel ab$  data is identical to  $\mu_{\text{eff}} = 3.41(5)\mu_B/\text{Cr}$  from  $H \parallel c$  data, which is close to the theoretical value expected for  $\text{Cr}^{3+}$  of  $3.87\mu_B$ . Figure 2(b) displays the isothermal magnetization measured at  $T = 2 \text{ K}$ . The saturation field  $H_s \approx 3000 \text{ Oe}$  for  $H \parallel c$  is smaller than  $H_s \approx 5000 \text{ Oe}$  for  $H \parallel ab$ , confirming the easy axis is the  $c$  axis. The saturation moment at  $T = 2 \text{ K}$  is  $M_s \approx 2.45(1)\mu_B/\text{Cr}$  for  $H \parallel ab$  and  $M_s \approx 2.39(1)\mu_B/\text{Cr}$  for  $H \parallel c$ , respectively, close to the expected value of  $3\mu_B$  for  $\text{Cr}^{3+}$  with three unpaired spins. The inset of Fig. 2(b) shows  $M(H)$  in the low-field region and the absence of coercive force ( $H_c$ ) for  $\text{Cr}_2\text{Ge}_2\text{Te}_6$ . All these results are in good agreement with previous reports [5,13].

The critical behavior of a second-order transition can be characterized in detail by a series of interrelated critical

exponents [26]. In the vicinity of a second-order phase transition, the divergence of correlation length  $\xi = \xi_0|(T - T_c)/T_c|^{-\nu}$  leads to universal scaling laws for the spontaneous magnetization  $M_s$  and the inverse initial magnetic susceptibility  $\chi_0^{-1}$ . The spontaneous magnetization  $M_s$  below  $T_c$ , the inverse initial susceptibility  $\chi_0^{-1}$  above  $T_c$ , and the measured magnetization  $M(H)$  at  $T_c$  are characterized by a set of critical exponents  $\beta$ ,  $\gamma$ , and  $\delta$ . The mathematical definitions of these exponents from magnetization are

$$M_s(T) = M_0(-\varepsilon)^\beta, \quad \varepsilon < 0, \quad T < T_c, \quad (1)$$

$$\chi_0^{-1}(T) = (h_0/m_0)\varepsilon^\gamma, \quad \varepsilon > 0, \quad T > T_c, \quad (2)$$

$$M = DH^{1/\delta}, \quad \varepsilon = 0, \quad T = T_c, \quad (3)$$

where  $\varepsilon = (T - T_c)/T_c$  is the reduced temperature, and  $M_0$ ,  $h_0/m_0$ , and  $D$  are the critical amplitudes [27]. The magnetic equation of state is a relationship among the variables  $M(H, \varepsilon)$ ,  $H$ , and  $T$ . Using the scaling hypothesis this can be expressed as

$$M(H, \varepsilon) = \varepsilon^\beta f_\pm(H/\varepsilon^{\beta+\gamma}), \quad (4)$$

where  $f_+$  for  $T > T_c$  and  $f_-$  for  $T < T_c$ , respectively, are the regular functions. In terms of renormalized magnetization  $m \equiv \varepsilon^{-\beta} M(H, \varepsilon)$  and renormalized field  $h \equiv \varepsilon^{-(\beta+\gamma)} H$ , Eq. (4) can be written as

$$m = f_\pm(h), \quad (5)$$

which implies that for true scaling relations and the right choice of  $\beta$ ,  $\gamma$ , and  $\delta$  values, scaled  $m$  and  $h$  will fall on two universal curves: one above  $T_c$  and another below  $T_c$ . This is an important criterion for the critical regime.

In order to clarify the nature of the PM-FM transition in  $\text{Cr}_2\text{Ge}_2\text{Te}_6$ , we measured the isothermal  $M(H)$  in the temperature range from  $T = 52$  to 68 K, as shown in Fig. 3(a). Generally, the conventional method to determine the critical exponents and critical temperature involves the use of an Arrott plot [28]. The Arrott plot assumes critical exponents following the mean-field theory with  $\beta = 0.5$  and  $\gamma = 1.0$  [28]. According to this method, isotherms plotted in the form of  $M^2$  vs  $H/M$  constitute a set of parallel straight lines, and the isotherm at the critical temperature  $T_c$  should pass through the origin. At the same time, it directly gives  $\chi_0^{-1}(T)$  and  $M_s(T)$  as the intercepts on the  $H/M$  axis and positive  $M^2$  axis, respectively. Figure 3(b) shows the Arrott plot. All the curves in this plot show nonlinear behavior having a downward curvature even in high fields. This suggests that the mean-field model is not valid for  $\text{Cr}_2\text{Ge}_2\text{Te}_6$ . According to Banerjee's criterion [29], one can estimate the order of the magnetic transition through the slope of the straight line: A negative slope corresponds to the first-order transition while positive corresponds to the second order. Therefore, the concave downward curvature clearly indicates the PM-FM transition in  $\text{Cr}_2\text{Ge}_2\text{Te}_6$  is a second-order one. We also examined other three-dimensional (3D) models, including a 3D Heisenberg ( $\beta = 0.365$ ,  $\gamma = 1.386$ ), 3D XY ( $\beta = 0.345$ ,  $\gamma = 1.316$ ), 3D Ising model ( $\beta = 0.325$ ,  $\gamma = 1.24$ ), and tricritical mean-field model ( $\beta = 0.25$ ,  $\gamma = 1.0$ ) [28,29]. As shown in Fig. 4, all these models failed to yield parallel straight lines, suggesting the breakdown of these 3D models.

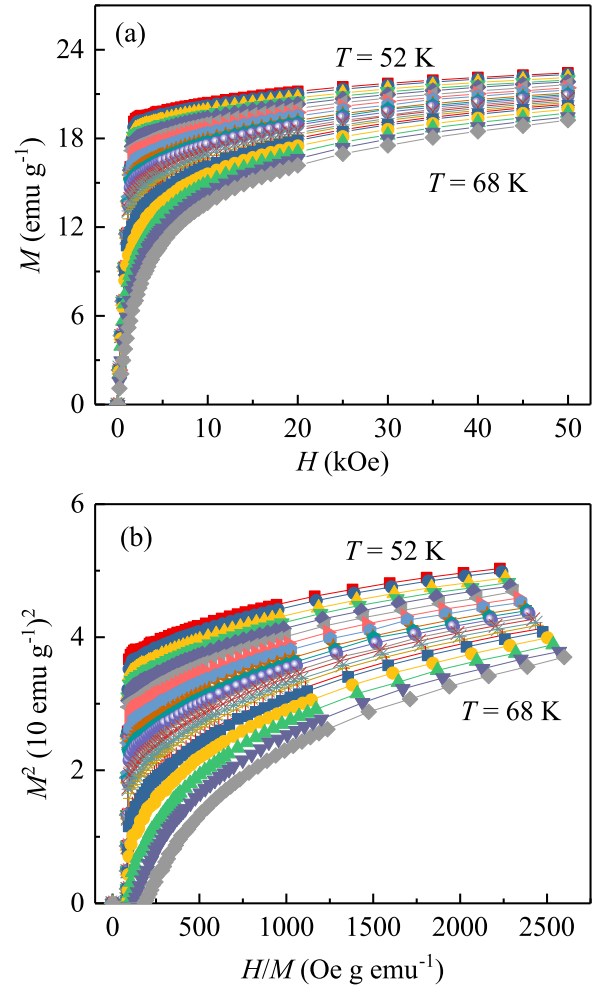


FIG. 3. (a) Typical initial isothermal magnetization curves from  $T = 52$  to 68 K for  $\text{Cr}_2\text{Ge}_2\text{Te}_6$ . (b) Arrott plots of  $M^2$  vs  $H/M$  around  $T_c$  for  $\text{Cr}_2\text{Ge}_2\text{Te}_6$ .

Considering the strong two-dimensional (2D) characteristics in  $\text{Cr}_2\text{Ge}_2\text{Te}_6$ , we further analyze the isothermal data with the 2D Ising model ( $\beta = 0.125$ ,  $\gamma = 1.75$ ) [30]. As shown in Fig. 5(a), a set of quasiparallel straight lines are obtained. However, there is still no single straight line that passes through the origin, indicating that  $\text{Cr}_2\text{Ge}_2\text{Te}_6$  cannot be rigorously described by the 2D Ising model. Therefore, a modified Arrott plot by a self-consistent method is further applied to determine  $T_c$  as well as the critical exponents  $\beta$  and  $\gamma$  [31]. The modified Arrott plot is given by the Arrot-Noaks equation of state

$$(H/M)^{1/\gamma} = a\varepsilon + bM^{1/\beta}, \quad (6)$$

where  $\varepsilon = (T - T_c)/T_c$  is the reduced temperature, and  $a$  and  $b$  are constants. To find out the proper values of  $\beta$  and  $\gamma$ , a rigorous iterative method has been used [32]. The starting values of  $M_s(T)$  and  $\chi_0^{-1}(T)$  were determined from the 2D Ising model plot by linear extrapolation from the high-field region to the intercepts with the axis  $M^{1/\beta}$  and  $(H/M)^{1/\gamma}$ , respectively. A new set of  $\beta$  and  $\gamma$  can be obtained by fitting the data following Eqs. (1) and (2). Then the obtained new values of  $\beta$  and  $\gamma$  are used to reconstruct a new modified Arrott plot. This procedure was repeated until the values of  $\beta$  and  $\gamma$

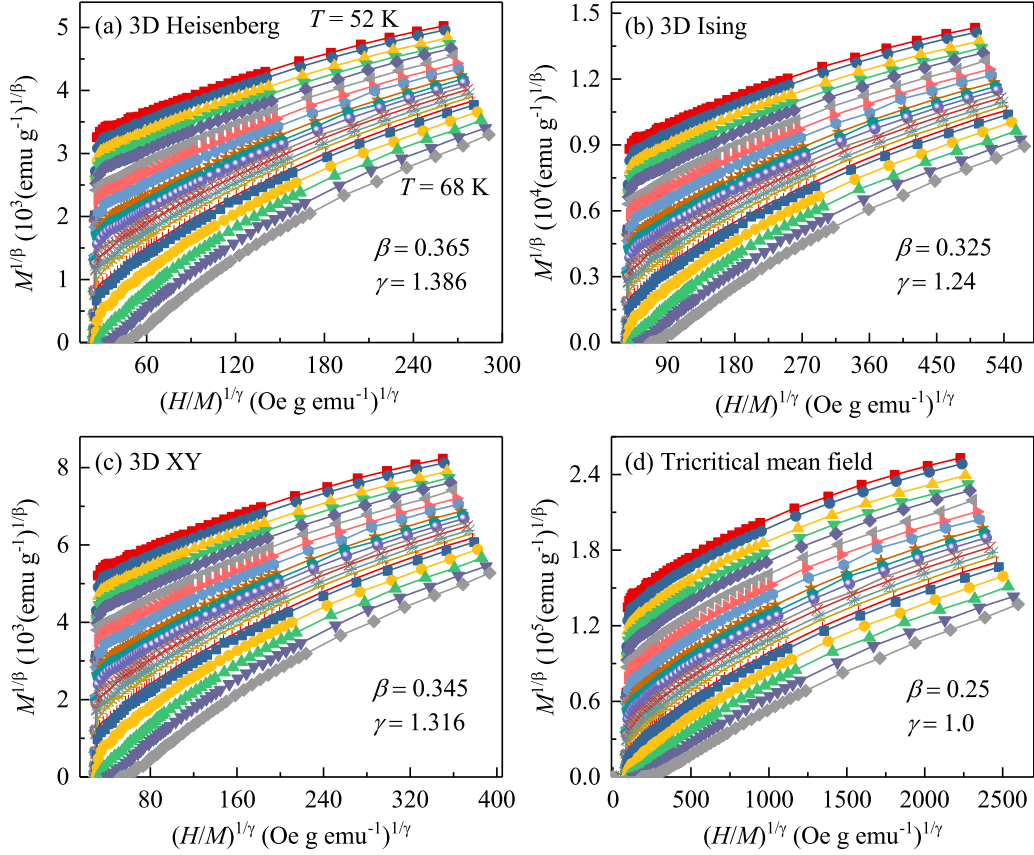


FIG. 4. The isotherms plotted as  $M^{1/\beta}$  vs  $(H/M)^{1/\gamma}$  with a (a) 3D Heisenberg model, (b) 3D Ising model, (c) 3D XY model, and (d) tricritical mean-field model.

are stable. By this method, the obtained critical exponents are hardly dependent on the initial parameters, which confirms these critical exponents are reliable and intrinsic. The final modified Arrott plots generated with the values  $\beta = 0.194$  and  $\gamma = 1.36$  are depicted in Fig. 5(b).

Figure 6(a) presents the final  $M_s(T)$  and  $\chi_0^{-1}(T)$  with solid fitting curves. The critical exponents  $\beta = 0.196(3)$  with  $T_c = 62.64(2)$  K and  $\gamma = 1.32(5)$  with  $T_c = 62.66(9)$  K are obtained, which are very close to the values obtained from the modified Arrott plot in Fig. 5(b). Alternatively, the critical exponents can be determined by the Kouvel-Fisher (KF) method [33],

$$\frac{M_s(T)}{dM_s(T)/dT} = \frac{T - T_c}{\beta}, \quad (7)$$

$$\frac{\chi_0^{-1}(T)}{d\chi_0^{-1}(T)/dT} = \frac{T - T_c}{\gamma}. \quad (8)$$

According to this method,  $M_s(T)/[dM_s(T)/dT]$  and  $\chi_0^{-1}(T)/[d\chi_0^{-1}(T)/dT]$  are as linear functions of temperature with slopes of  $1/\beta$  and  $1/\gamma$ , respectively. As shown in Fig. 6(b), the linear fits give  $\beta = 0.200(3)$  with  $T_c = 62.65(7)$  K and  $\gamma = 1.28(3)$  with  $T_c = 62.75(6)$  K, respectively.

Isothermal magnetization  $M(H)$  at a critical temperature  $T_c = 62.7$  K is shown in Fig. 7, with the inset plotted on a log-log scale. According to Eq. (3), the third critical exponent  $\delta = 7.96(1)$  can be deduced. Furthermore, the exponent  $\delta$  can also

been calculated from the Widom scaling relation according to which critical exponents  $\beta$ ,  $\gamma$ , and  $\delta$  are related in the following way,

$$\delta = 1 + \frac{\gamma}{\beta}. \quad (9)$$

Using the  $\beta$  and  $\gamma$  values determined from the modified Arrott plot and Kouvel-Fisher plot, we obtain  $\delta = 7.73(15)$  and  $\delta = 7.40(5)$ , respectively, which are very close to the value obtained from a critical isotherm analysis.

The reliability of the obtained critical exponents and  $T_c$  can also be verified by a scaling analysis. Following Eq. (5), scaled  $m$  versus scaled  $h$  has been plotted in Fig. 7(a), along with the same plot on a log-log scale in the inset of Fig. 8(a). It is rather significant that all the data collapse into two separate branches, one below  $T_c$  and another above  $T_c$ . The reliability of the exponents and  $T_c$  has been further ensured with a more rigorous method by plotting  $m^2$  vs  $h/m$ , as shown in Fig. 8(b), where all data also fall on two independent branches. This clearly indicates that the interactions get properly renormalized in a critical regime following the scaling equation of state. In addition, the scaling equation of state takes another form,

$$\frac{H}{M^\delta} = k\left(\frac{\varepsilon}{H^{1/\beta}}\right), \quad (10)$$

where  $k(x)$  is the scaling function. Based on Eq. (10), all experimental curves will collapse onto a single curve. The inset



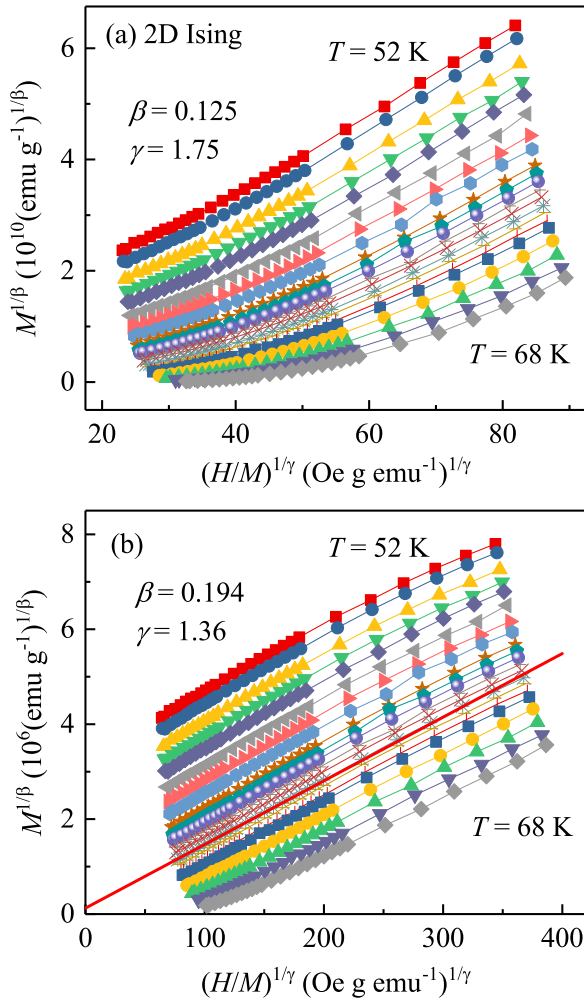


FIG. 5. (a) 2D Ising model plot of isotherms for  $\text{Cr}_2\text{Ge}_2\text{Te}_6$ . (b) Modified Arrott plot of  $M^{1/\beta}$  vs  $(H/M)^{1/\gamma}$  with  $\beta = 0.194$  and  $\gamma = 1.36$  for  $\text{Cr}_2\text{Ge}_2\text{Te}_6$ . The straight line is the linear fit of the isotherm at  $T = 62.5$  K.

of Fig. 8(b) shows the  $MH^{-1/\delta}$  vs  $\varepsilon H^{-1/(\beta\delta)}$  for  $\text{Cr}_2\text{Ge}_2\text{Te}_6$ , where the experimental data collapse onto a single curve, and  $T_c$  locates at the zero point of the horizontal axis. The well-rescaled curves further confirm the reliability of the obtained critical exponents. All critical exponents derived from various methods are given in Table I along with the values of  $\text{Cr}_2\text{Si}_2\text{Te}_6$  and the theoretically predicted values for different models. As we can see, the experimentally determined critical exponents  $\beta$ ,  $\gamma$ , and  $\delta$  are close to but show some deviation from the theoretical values of the 2D Ising model, which might be associated with non-negligible interlayer coupling and spin-lattice coupling in this material [10,21]. Compared to  $\text{Cr}_2\text{Si}_2\text{Te}_6$  [ $\beta = 0.175(9)$ ,  $\gamma = 1.562(9)$ ], the critical exponents [ $\beta = 0.200(3)$ ,  $\gamma = 1.28(3)$ ] for  $\text{Cr}_2\text{Ge}_2\text{Te}_6$  can be explained by larger  $\text{Ge}_2\text{Te}_6$  octahedra and a smaller van der Waals (vdW) gap that induced stronger interlayer coupling in  $\text{Cr}_2\text{Ge}_2\text{Te}_6$ .

Finally, we would like to discuss the nature as well as the range of interactions in  $\text{Cr}_2\text{Ge}_2\text{Te}_6$ . For a homogeneous magnet, the universality class of the magnetic phase transition depends on the exchange distance  $J(r)$ . Fisher *et al.* theoretically treated this kind of magnetic ordering as an attractive

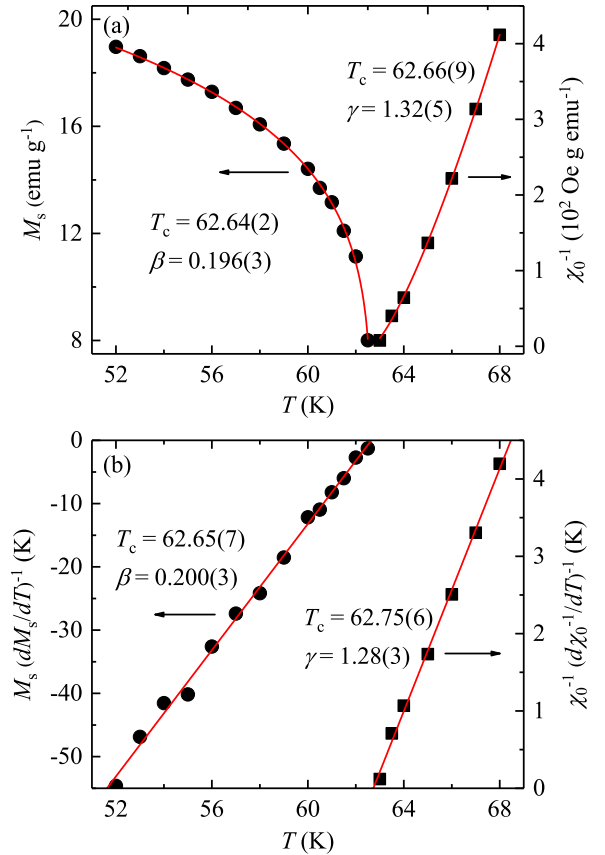


FIG. 6. (a) Temperature dependence of the spontaneous magnetization  $M_s$  (left) and the inverse initial susceptibility  $\chi_0^{-1}$  (right) with solid fitting curves for  $\text{Cr}_2\text{Ge}_2\text{Te}_6$ . (b) Kouvel-Fisher plots of  $M_s(dM_s/dT)^{-1}$  (left) and  $\chi_0^{-1}(d\chi_0^{-1}/dT)^{-1}$  (right) with solid fitting curves for  $\text{Cr}_2\text{Ge}_2\text{Te}_6$ .

interaction of spins, where a renormalization group theory analysis suggests the interaction decays with distance  $r$  as

$$J(r) \approx r^{-(d+\sigma)}, \quad (11)$$

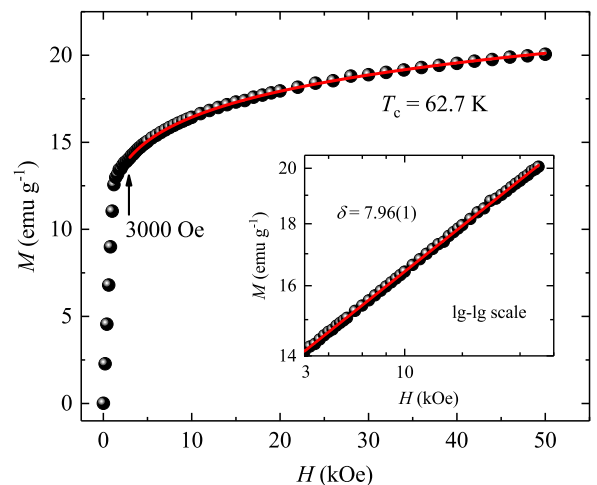


FIG. 7. Isotherm  $M$  vs  $H$  plot collected at  $T_c = 62.7$  K for  $\text{Cr}_2\text{Ge}_2\text{Te}_6$ . Inset: The same plot in log-log scale with a solid fitting curve.

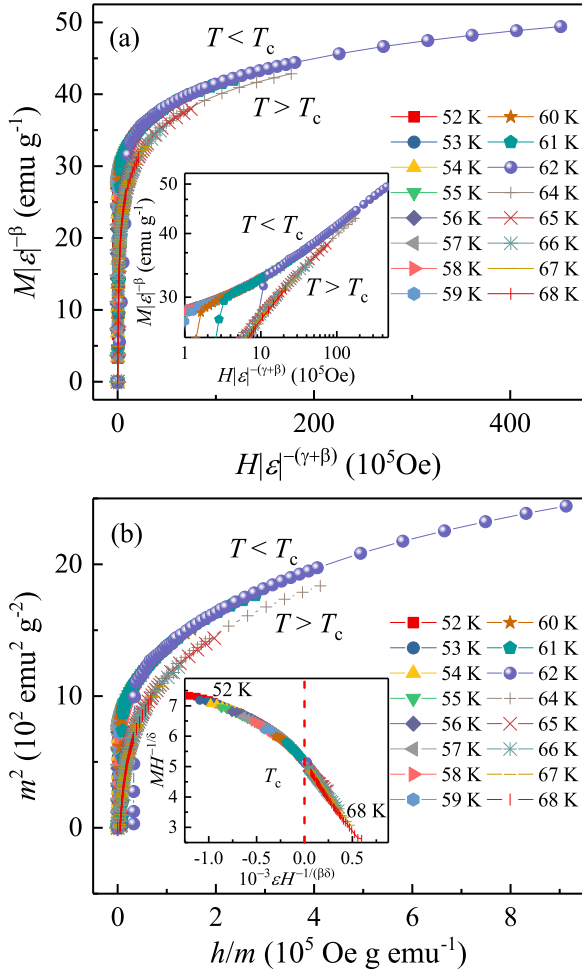


FIG. 8. (a) Scaling plots of renormalized magnetization  $m$  vs renormalized field  $h$  below and above  $T_c$  for  $\text{Cr}_2\text{Ge}_2\text{Te}_6$ . Inset: The same plots in log-log scale. (b) The renormalized magnetization and field replotted in the form of  $m^2$  vs  $h/m$  for  $\text{Cr}_2\text{Ge}_2\text{Te}_6$ . Inset: The rescaling of the  $M(H)$  curves by  $MH^{-1/\delta}$  vs  $\epsilon H^{-1/(\beta\delta)}$ .

where  $d$  is the spatial dimensionality and  $\sigma$  is a positive constant [34]. According to this model, the range of the spin interaction is long or short depending on  $\sigma < 2$  or  $\sigma > 2$ , and it predicts the susceptibility exponent  $\gamma$  which has been calculated from a renormalization group approach,

as follows,

$$\gamma = 1 + \frac{4}{d} \left( \frac{n+2}{n+8} \right) \Delta\sigma + \frac{8(n+2)(n-4)}{d^2(n+8)^2} \times \left[ 1 + \frac{2G(\frac{d}{2})(7n+20)}{(n-4)(n+8)} \right] \Delta\sigma^2, \quad (12)$$

where  $\Delta\sigma = (\sigma - \frac{d}{2})$  and  $G(\frac{d}{2}) = 3 - \frac{1}{4}(\frac{d}{2})^2$ . To find out the range of interaction ( $\sigma$ ) as well as the dimensionality of both the lattice ( $d$ ) and spin ( $n$ ) in this system we have followed the procedure similar to Ref. [35], where the parameter  $\sigma$  in the above expression is adjusted for particular values of  $\{d : n\}$  so that it yields a value for  $\gamma$  close to that experimentally observed,  $\gamma = 1.28$ . The so obtained  $\sigma$  is then used to calculate the remaining exponents from the following expressions:  $\nu = \gamma/\sigma$ ,  $\alpha = 2 - \nu d$ ,  $\beta = (2 - \alpha - \gamma)/2$ , and  $\delta = 1 + \gamma/\beta$ . This exercise is repeated for a different set of  $\{d : n\}$ . We found that  $\{d : n\} = \{2 : 1\}$  and  $\sigma = 1.52$  give the exponents ( $\beta = 0.256$ ,  $\gamma = 1.617$ , and  $\delta = 7.32$ ) which are close to our experimentally observed values (Table I). This calculation suggests the spin interaction in  $\text{Cr}_2\text{Ge}_2\text{Te}_6$  is of a 2D Ising ( $\{d : n\} = \{2 : 1\}$ ) type coupled with a long-range ( $\sigma = 1.52$ ) interaction.

#### IV. CONCLUSIONS

In summary, we have made a comprehensive study of the critical behavior at the PM-FM phase transition in the quasi-2D semiconducting ferromagnet  $\text{Cr}_2\text{Ge}_2\text{Te}_6$ . This transition is identified to be second order in nature. The critical exponents  $\beta$ ,  $\gamma$ , and  $\delta$  estimated from various techniques match reasonably well and follow the scaling equation, confirming that the obtained exponents are unambiguous and intrinsic to the material. The determined exponents match well with those calculated from the results of the renormalization group approach for a 2D Ising ( $\{d : n\} = \{2 : 1\}$ ) system coupled with a long-range interaction between spins decaying as  $J(r) \approx r^{-(d+\sigma)}$  with  $\sigma = 1.52$ .

*Note added.* Recently, we became aware that Lin *et al.* [36] also synthesized  $\text{Cr}_2\text{Ge}_2\text{Te}_6$ . Their conclusions regarding the tricritical point [ $\beta = 0.240(6)$ ,  $\gamma = 1.000(5)$ ,  $\delta = 5.070(6)$ ,  $T_c = 67.9$  K] obtained by fitting in a different field range are not in conflict with our work [ $\beta = 0.200(3)$ ,  $\gamma = 1.28(3)$ ,

TABLE I. Comparison of critical exponents of  $\text{Cr}_2\text{Ge}_2\text{Te}_6$  and  $\text{Cr}_2\text{Si}_2\text{Te}_6$  with different theoretical models.

Composition	Reference	Technique	$\beta$	$\gamma$	$\delta$
$\text{Cr}_2\text{Ge}_2\text{Te}_6$	This work	Modified Arrott plot	0.196(3)	1.32(5)	7.73(15)
	This work	Kouvel-Fisher plot	0.200(3)	1.28(3)	7.40(5)
	This work	Critical isotherm			7.96(1)
$\text{Cr}_2\text{Si}_2\text{Te}_6$	[22]	Kouvel-Fisher plot	0.175(9)	1.562(9)	9.925(56)
2D Ising	[30]	Theory	0.125	1.75	15
Mean field	[28]	Theory	0.5	1.0	3.0
3D Heisenberg	[28]	Theory	0.365	1.386	4.8
3D XY	[28]	Theory	0.345	1.316	4.81
3D Ising	[28]	Theory	0.325	1.24	4.82
Tricritical mean field	[29]	Theory	0.25	1.0	5

$\delta = 7.96(1)$ ,  $T_c = 62.7$  K] that are deduced from fitting in the field range from 5 to 50 kOe for a modified Arrott plot and from 3 to 50 kOe for a critical isotherm at  $T_c = 62.7$  K, respectively.

## ACKNOWLEDGMENTS

This work was supported by the US Department of Energy, Office of Basic Energy Sciences as part of the Computational Material Science Program.

- 
- [1] Q. H. Wang, K. Kalantar-Zadeh, A. Kis, J. N. Coleman, and M. S. Strano, *Nat. Nanotechnol.* **7**, 699 (2012).
- [2] A. K. Geim and I. V. Grigorieva, *Nature (London)* **499**, 419 (2013).
- [3] S. Lebègue, T. Björkman, M. Klintonberg, R. M. Nieminen, and O. Eriksson, *Phys. Rev. X* **3**, 031002 (2013).
- [4] C. Gong, L. Li, Z. L. Li, H. W. Ji, A. Stern, Y. Xia, T. Cao, W. Bao, C. Z. Wang, Y. Wang, Z. Q. Qiu, R. J. Cava, S. G. Louie, J. Xia, and X. Zhang, *Nature (London)* **546**, 265 (2017).
- [5] H. W. Ji, R. A. Stokes, L. D. Aegria, E. C. Blomberg, M. A. Tanatar, A. Reijnders, L. M. Schoop, T. Liang, R. Prozorov, K. S. Burch, N. P. Ong, J. R. Petta, and R. J. Cava, *J. Appl. Phys.* **114**, 114907 (2013).
- [6] B. Sachs, T. O. Wehling, K. S. Novoselov, A. I. Lichtenstein, and M. I. Katsnelson, *Rhys. Rev. B* **88**, 201402 (2013).
- [7] I. Yamada, *J. Phys. Soc. Jpn.* **33**, 979 (1972).
- [8] H. Kabbour, R. David, A. Pautrat, H. J. Koo, M. H. Whangbo, G. André, and O. Mentré, *Angew. Chem., Int. Ed.* **51**, 11745 (2012).
- [9] M. A. McGuire, H. Dixit, V. R. Cooper, and B. C. Sales, *Chem. Mater.* **27**, 612 (2015).
- [10] L. D. Casto, A. J. Clune, M. O. Yokosuk, J. L. Musfeldt, T. J. Williams, H. L. Zhuang, M. W. Lin, K. Xiao, R. G. Hennig, B. C. Sales, J. Q. Yan, and D. Mandrus, *APL Mater.* **3**, 041515 (2015).
- [11] X. Zhang, Y. L. Zhao, Q. Song, S. Jia, J. Shi, and W. Han, *Jpn. J. Appl. Phys.* **55**, 033001 (2016).
- [12] V. Carreaux, G. Ouvrard, J. C. Grenier, and Y. Laligant, *J. Magn. Magn. Mater.* **94**, 127 (1991).
- [13] V. Carreaux, D. Brunet, G. Ouvrard, and G. André, *J. Phys.: Condens. Matter* **7**, 69 (1995).
- [14] G. Ouvrard, E. Sandre, and R. Brec, *J. Solid State Chem.* **73**, 27 (1988).
- [15] B. Siberchicot, S. Jobic, V. Carreaux, P. Gressier, and G. Ouvrard, *J. Phys. Chem.* **100**, 5863 (1996).
- [16] X. X. Li and J. L. Yang, *J. Mater. Chem. C* **2**, 7071 (2014).
- [17] X. F. Chen, J. S. Qi, and D. N. Shi, *Phys. Lett. A* **379**, 60 (2015).
- [18] N. Sivadas, M. W. Daniels, R. H. Swendsen, S. Okamoto, and D. Xiao, *Phys. Rev. B* **91**, 235425 (2015).
- [19] J. P. Liu, S. Y. Park, K. F. Garrity, and D. Vanderbilt, *Phys. Rev. Lett.* **117**, 257201 (2016).
- [20] M. W. Lin, H. L. Zhuang, J. Q. Yan, T. Z. Ward, A. A. Puretzky, C. M. Rouleau, Z. Gai, L. B. Liang, V. Meunier, B. G. Sumpter, P. Ganesh, P. R. C. Kent, D. B. Geohegan, D. G. Mandrus, and K. Xiao, *J. Mater. Chem. C* **4**, 315 (2016).
- [21] V. Carreaux, F. Moussa, and M. Spiesser, *Europhys. Lett.* **29**, 251 (1995).
- [22] B. J. Liu, Y. M. Zou, L. Zhang, S. M. Zhou, Z. Wang, W. K. Wang, Z. Qu, and Y. H. Zhang, *Sci. Rep.* **6**, 33873 (2016).
- [23] T. J. Williams, A. A. Aczel, M. D. Lumsden, S. E. Nagler, M. B. Stone, J. Q. Yan, and D. Mandrus, *Phys. Rev. B* **92**, 144404 (2015).
- [24] N. D. Mermin and H. Wagner, *Phys. Rev. Lett.* **17**, 1133 (1966).
- [25] H. L. Zhuang, Y. Xie, P. R. C. Kent, and P. Ganesh, *Phys. Rev. B* **92**, 035407 (2015).
- [26] H. E. Stanley, *Introduction to Phase Transitions and Critical Phenomena* (Oxford University Press, London, 1971).
- [27] M. E. Fisher, *Rep. Prog. Phys.* **30**, 615 (1967).
- [28] A. Arrott, *Phys. Rev.* **108**, 1394 (1957).
- [29] S. K. Banerjee, *Phys. Lett.* **12**, 16 (1964).
- [30] J. C. LeGuillou and J. Zinn-Justin, *Phys. Rev. B* **21**, 3976 (1980).
- [31] A. Arrott and J. Noakes, *Phys. Rev. Lett.* **19**, 786 (1967).
- [32] A. K. Pramanik and A. Banerjee, *Phys. Rev. B* **79**, 214426 (2009).
- [33] J. S. Kouvel and M. E. Fisher, *Phys. Rev.* **136**, A1626 (1964).
- [34] M. E. Fisher, S. K. Ma, and B. G. Nickel, *Phys. Rev. Lett.* **29**, 917 (1972).
- [35] S. F. Fischer, S. N. Kaul, and H. Kronmuller, *Phys. Rev. B* **65**, 064443 (2002).
- [36] G. T. Lin, H. L. Zhuang, X. Luo, B. J. Liu, F. C. Chen, J. Yan, Y. Sun, J. Zhou, W. J. Lu, P. Tong, Z. G. Sheng, Z. Qu, W. H. Song, X. B. Zhu, and Y. P. Sun, *arXiv:1706.03239*.